Nitrate Radical Cannot Initiate Oxidation of Hg(0) to Hg(II) in the Laboratory or at Ground Level in the Atmosphere

Darshi T. Hewa Edirappulige,[1] Lan Cheng,[2] Pedro J. Castro,[1] and Theodore S. Dibble[1]

[1] Department of Chemistry, State University of New York, College of Environmental Science and Forestry, Syracuse, NY, 13210, U.S.A.

[2] Department of Chemistry, The Johns Hopkins University, Baltimore, Maryland 21218, U.S.A.

Correspondence to: Theodore S. Dibble (tsdibble@esf.edu)

Abstract. Multiple field studies have led to suggestions that nitrate radical (NO_3) participates in oxidizing gaseous $Hg^{(0)}$ in the atmosphere. These suppositions are hard to reconcile with the two-step mechanism of $Hg^{(0)}$ conversion to $Hg^{(II)}$ via $Hg^{(I)}$, due to the instability of the NO_3-$Hg^{(I)}$. We use a high level of computational chemistry to determine its bond energy as 6.5 kcal mol^{-1}. We use statistical mechanics to compute the equilibrium constant, $K_c(T)$ for $NO_3 + Hg^{(0)} = NO_3Hg^{(I)}$, and a box model to investigate a field study and laboratory kinetic investigation of this chemistry. Under the conditions of the one field study showing a correlation between $[NO_3]$ and $[Hg^{(II)}(g)]$, NO_3 could not have contributed significantly to the formation of $Hg^{(II)}$. In addition, we find that the one experimental kinetic study of this reaction does not constrain the rate constant.

1 Introduction

The atmosphere transports gaseous elemental mercury ($Hg^{(0)}$, GEM) globally, so that this neurotoxic pollutant is found in the poles as well as near its emission sources (Schroeder and Munthe, 1998). GEM deposits from the gaseous atmosphere roughly equally into vegetation versus oceans, in competition with reacting to form gaseous oxidized mercury (GOM), that is, $Hg^{(II)}$ (Shah et al., 2021; Zhou and Obrist, 2021). GOM, if not reduced back to GEM (Saiz-Lopez et al., 2018; Wu et al., 2022), will deposit predominantly into oceans. The contrasting fates of GEM and GOM means that we need to understand the redox chemistry of atmospheric mercury to predict when and where mercury enters ecosystems.

Gas-phase oxidation of GEM to GOM in the tropopshere and lower stratosphere occurs via addition of a radical (Br, OH, or Cl) to form a mercury-centered radical form of $Hg^{(I)}$, which is further oxidized to $Hg^{(II)}$ by reaction with ozone (Castro et al., 2022; Gómez Martín et al., 2022), NO_2, HOO, or most other radicals (Dibble et al., 2012, 2013, 2020; Goodsite, M. E. Plane and Skov, 2004; Horowitz et al., 2017; Shah et al., 2021; Wang et al., 2014; Wu et al., 2024, 2020). Production of Br, OH, and Cl falls dramatically around sunset, so this mechanism does not explain multiple observations of elevated [GOM] at night. During nighttime, nitrate radical (NO_3) is the major oxidant for most volatile organic compounds (Brown and Stutz, 2012), so, naturally, atmospheric scientists have invoked NO_3 to explain elevated [GOM] at night (Mao et al., 2008; Peleg et al., 2015; Weiss-Penzias et al., 2003). Peleg et al. (2015) presented the most compelling evidence, namely, a strong correlation between

measured nightime [GOM] and [NO_3] in Jerusalem over the course of six weeks. Unfortunately, there is very little kinetic or thermodynamic data to support these suggestions. Sommar et al. (1997) reported an upper limit to the reaction:

$$Hg + NO_3 \rightarrow \text{Products} \quad (1)$$

at room temperature of $k_1 \leq 4 \times 10^{-15}$ cm^3 molecule^{-1} s^{-1} from flow-tube experiments. Sumner et al., (2005) reported $k_1 \leq 7 \times 10^{-15}$ cm^3 molecule^{-1} s^{-1} from a chamber experiment. As noted by Hynes et al. (2009), production of $Hg^{(I)}O + NO_2$ in reaction (1) had subsequently been revealed to be highly endothermic (by ~45 kcal mol^{-1}). As a result, it seems more likely that reaction (1) proceeds via formation of an adduct:

$$Hg + NO_3 + M \leftrightarrows NO_3Hg^{(I)}\bullet + M \quad (2)$$

(where M is a third body) mimicking the mechanism for other radicals:

$$Hg^{(0)} + Y + M \leftrightarrows YHg^{(I)}\bullet + M \quad (Y = Br, OH, Cl) \quad (3)$$

However, quantum calculations by Dibble et al. (2012) indicated that $NO_3Hg^{(I)}\bullet$ was very weakly bound (5.0 kcal mol^{-1} at 0 K). At the time, the only known pathway for oxidation of $NO_3Hg^{(I)}\bullet$ was, as for other $YHg^{(I)}\bullet$, via addition of radicals, $\bullet Z$ (Z = NO_2, HOO, halogen oxides, etc., but not NO):

$$NO_3Hg^{(I)}\bullet + \bullet Z + M \rightarrow NO_3Hg^{(II)}Z + M \quad (4)$$

The weak bonding of $NO_3Hg^{(I)}\bullet$ and the low concentrations of radicals, $\bullet Z$, in the atmosphere led Dibble et al. (2012) to conclude that NO_3 could not initiate oxidation of GEM to GOM.

The subsequent report, by Peleg et al. (2015) of a strong correlation between [NO_3] and [GOM] led us to consider two caveats to the conclusion of Dibble et al (2012). First, NO_3 radical is rather challenging for quantum chemistry, and the previous calculations could easily be improved upon. Second, it had subsequently been determined that $YHg^{(I)}\bullet$ could react with ozone with a high rate constant (Castro et al., 2022; Gómez Martín et al., 2022), via:

$$YHg^{(I)}\bullet + O_3 \rightarrow YHg^{(II)}O\bullet + O_2 \quad (5)$$

In the case of $HOHg^{(I)}\bullet$, with a bond energy at 0 K (D_0) of 11.0 kcal mol^{-1} (Dibble et al., 2020), the abundance of ozone and the high rate constant for reaction (5) enables OH to contribute significantly (~30%) to global production of GOM from GEM (Shah et al., 2021). Without reaction (5), Dibble et al. (2020) concluded that OH would contribute < 1% to GEM oxidation. Typical nighttime [NO_3] is perhaps 20-100 times higher than typical daytime [OH] (Chua et al., 2023; Khan et al., 2015; Penkett et al., 2007), and this higher concentration could enable NO_3 to initiate oxidation of GEM even though the NO_3-$Hg^{(I)}$ bond energy was likely lower that the HO-$Hg^{(I)}$ bond energy.

Below we discuss the theoretical methods for our calculations. We then report the structure and bond energy of $NO_3Hg^{(I)}\bullet$, followed by the equilibrium constant of reaction (2) versus temperature. Next, we use these results to evaluate the reliability of the upper limit to k_2 reported by Sommar et al. (1997). We then determine whether NO_3-initiated oxidation of GEM can explain the observations of Peleg et al. (2015). Finally, we briefly consider the potential for NO_3 to play a major role in GEM oxidation the atmosphere, more generally.

2 Methods

Our calculations aim at an accurate D_0 for $NO_3Hg^{(I)}$• to accurately calculate the equilibrium constant for reaction (2). The electronic structure of NO_3 poses major challenges on quantum chemistry calculations because of the multireference characters and symmetry breaking due to pseudo-Jahn-Teller coupling in its open-shell electronic states (Eisfeld and Morokuma, 2000; Stanton et al., 1991; Viel and Eisfeld, 2018). On the other hand, the NO_3^- anion has a simple closed-shell electronic ground state. Equation-of-motion ionization potential coupled-cluster (EOMIP-CC) calculations (Stanton and Bartlett, 1993; Stanton and Gauss, 1994) using the closed-shell ground state of NO_3^- as the reference state and removing an electron to obtain NO_3 has been shown to accurately describe low-lying electronic states of NO_3 (Stanton, 2007, 2009). We follow this prescription here and perform calculations of NO_3 and $HgNO_3^{(I)}$• using the EOMIP-CC singles and double (CCSD) and CC singles doubles triples (CCSDT) methods (Matthews and Stanton, 2015; Stanton and Gauss, 1999). The spin-free exact two-component theory in its one-electron variant (the SFX2C-1e scheme) (Cheng and Gauss, 2011; Dyall, 2001; Liu and Peng, 2009) has been used to treat the scalar-relativistic effect. The equilibrium structures and harmonic vibrational frequencies of NO_3 and $NO_3Hg^{(I)}$• have been calculated with the valence electrons correlated using triple-zeta quality atomic natural orbital (ANORCC1) basis sets using the primitive functions of the ANO-RCC sets (Faegri Jr, 2001; Roos et al., 2003, 2005) recontracted for the SFX2C-1e calculations using CCSD density matrices. We have performed calculations of harmonic vibrational frequencies to confirm that the optimized structure corresponds to a stable structure on the potential energy surface.

To an obtain an accurate value of D_0, we carried out EOMIP-CCSD calculations with more complete treatments of basis-set and electron-correlation effects. These calculations have correlated valence and semicore electrons including the Hg 4f5s5p5d, N 2s2p, and O 2s2p electrons. We used uncontracted triple-zeta (TZ) and quadruple-zeta (QZ) basis sets for Hg constructed using primitive functions of the ANO-RCC sets and correlation-consistent sets (Peterson and Puzzarini, 2005) as well as aug-cc-pVTZ and aug-cc-pVQZ sets for N and O (Kendall et al., 1992) recontracted for the SFX2C-1e scheme. The basis-set-limit (∞Z) EOMIP-CCSD energies were obtained by combining the QZ Hartree-Fock energies with basis-set-limit values for the EOMIP-CCSD electron-correlation and ionization energies estimated by extrapolating the TZ and QZ results using a simple two-point formula (Helgaker et al., 1997). The contributions due to the correlation of deep inner-shell electrons were estimated by performing EOMIP-CCSD/TZ calculations with the correlation of Hg 4s, 4p, 4d and O 1s orbitals. Furthermore, the contributions from triple excitations were obtained as the differences between EOMIP-CCSDT and CCSD results using the ANORCC1 basis sets. We also carried out EOMIP-CCSD calculations with spin-orbit coupling to obtain the second-order spin-orbit (SO) contributions to D_0. Here the X2C Hamiltonian (Dyall, 2001; Kutzelnigg and Liu, 2005; Liu and Peng, 2009) with atomic mean field (Heß et al., 1996) integrals (the X2CAMF scheme) (Liu and Cheng, 2018; Zhang and Cheng, 2022) has been used to provide variational treatments of spin-orbit coupling. We have used the recent implementation of the X2CAMF EOM excitation energy (EOMEE)-CCSD method (Asthana et al., 2019) together with the continuum orbital trick (Stanton and Gauss, 1999) for these X2CAMF-EOMIP calculations. The SO contribution to D_0 obtained from these calculations is less than 0.1 kcal/mol and thus insignificant for the present discussion. The basis sets used in the calculations

described here are documented in the Supporting Information. All calculations were performed using the CFOUR program package (Stanton et al..; Matthews et al., 2020). We calculated the equilibrium constant for reaction (2) vs. temperature (200-320 K) from D_0 with the *thermo* program in the MultiWell program suite (Barker, 2001, 2009; Barker et al., 2023), using the rigid rotor-harmonic oscillator approximation.

Our goal for understanding the oxidation of $NO_3Hg^{(I)}$• by radicals (NO_2, HOO, BrO, NO_3, and O_2) and ozone is to verify that these reactions occur similarly to those of $HOHg^{(I)}$• and $BrHg^{(I)}$•. While this requires reliable levels of theory, it does not require the precision needed in determining D_0. These quantum chemistry calculations used Gaussian16 (Frisch et al., 2016) and ORCA 5.0.3 (Neese, 2012, 2022). Density functional theory (DFT) was used to optimize geometries and compute harmonic vibrational frequencies. We used three functionals that have proven reliable in our previous studies of mercury chemistry: CAM-B3LYP (Yanai et al., 2004) with D3BJ dispersion correction (Grimme et al., 2011), PBE0 (Adamo and Barone, 1999), and M06-2X (Zhao and Truhlar, 2008). For H, N, and O atoms we used Dunning's aug-cc-pVTZ basis set (Dunning, 1989; Peterson and Dunning, 2002). To account for scalar relativistic effects in Hg and Br we used the Stuttgart/Cologne small-core pseudopotentials (ECPMDF60 and ECPMDF10, respectively) while the electrons outside the pseudopotential were described with the aug-cc-pVTZ-PP basis set of Peterson and co-workers (Figgen et al., 2005; Peterson et al., 2003; Peterson and Puzzarini, 2005). Our shorthand for this combination of basis sets is AVTZ. All radicals were treated with spin-unrestricted wavefunctions, and we verified the stability of wavefunctions. Spin orbit corrections to relative energies should be modest (< 1 kcal mol^{-1}) except for reactions involving BrO (Dixon et al., 2000; Jiao and Dibble, 2015).

3 Results and Discussion

3.1 Hg binding to NO_3 radical

We initially optimized a C_{2v} structure of $NO_3Hg^{(I)}$•, but this turned out to be a transition state (denoted TS-$NO_3Hg^{(I)}$•) at both DFT/AVTZ (for all three functionals) and SFX2C-1e-EOMIP-CCSD(T)/ANORCC1 levels. Instead, $NO_3Hg^{(I)}$• adopts a structure of C_s symmetry with the Hg atom binding asymmetrically (2.20 vs 2.56 Å) to two O atoms of NO_3 (see Fig. 1). Vibrational frequencies are listed in Tables S3 and S4 of the Supporting Information.

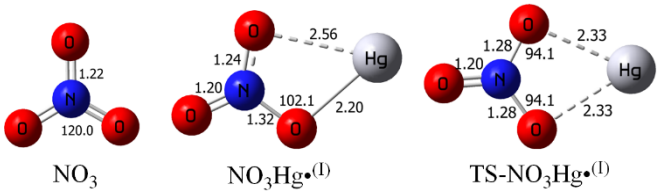

Figure 1. Structures of NO_3 (D_{3h}), $NO_3Hg^{(I)}$• (C_s), and TS-$NO_3Hg^{(I)}$• (C_{2v}) at SFX2C-1e-EOMIP-CCSD/ANORCC1 level. Angles and bond distances are listed in degrees and Å, respectively.

We computed the NO_3–Hg bond energy at 0 K (D_0) as 6.5 kcal mol^{-1}, which is 1.5 kcal mol^{-1} higher than the value computed previously. There are multiple possible contributions to this difference, including that Dibble et al. (2012) used lower levels of theory for structures (B3LYP vs EOMIP-CCSD) and energies (CCSD(T) vs CCSDT), and smaller basis sets for the energy evaluation (triple-zeta versus quadruple zeta extrapolated to the basis set limit).

As shown in Table S2, the difference between the D_0 values obtained from ∞Z and QZ calculations is about 1 kcal mol^{-1}. The remaining basis-set effects are likely substantially smaller. The contribution to D_0 from the correlation of the inner-shell electrons is around 0.5 kcal mol^{-1}. The remaining errors due to the correlation of even deeper electrons are expected to be insignificant. The triples contribution to D_0 amounts to around 0.5 kcal mol^{-1}. The remaining electron-correlation contributions due to quadruple excitations is expected to be smaller than the triples contributions. Based on the trends in these results, we estimate the uncertainty in the contribution from electronic energies to the value of D_0 to be about 1 kcal mol^{-1}.

Note that the NO_3 molecule exhibit complex vibronic structures because of the strong vibronic coupling between the ground ($\tilde{X}$) and second electronic excited ($\tilde{B}$) states of NO_3 (Eisfeld and Morokuma, 2000; Stanton, 2007, 2009; Viel and Eisfeld, 2018). The present calculations of the zero-point vibrational energy (ZPE) contribution to the bond energy used the harmonic vibrational frequencies given in Table S3 and S4. Viel and Eisfeld (2018) computed the anharmonic vibrational frequencies of NO_3 while accounting for $\tilde{X}$-$\tilde{B}$ vibronic coupling. They computed the ZPE as 6.8 kcal mol^{-1}, 0.2 kcal mol^{-1} smaller than our value of 7.0 kcal mol^{-1}. To compare directly with their value, we need to correct our $NO_3Hg^{(I)}$• results for anharmonicity. We did this using vibrational second-order perturbation theory (Mills, 1972) and obtained an anharmonic contribution of -0.1 kcal mol^{-1} to the ZPE of NO_3Hg. This means that our ZPE is 6.9 kcal mol^{-1}, or just 0.1 kcal mol^{-1} higher than obtained by Viel and Eisfeld (2018).

Table 1 lists the values of K_c for reaction (2) in the range 200 K ≤ T ≤ 320 K. We fit the values in Table 1 to an Arrhenius expression:

$$K_c = 1.0 \times 10^{-24}\ e^{3305/T}\ \text{cm}^3\ \text{molecule}^{-1} \qquad (6)$$

with less than 1% deviation from the values in Table 1. Because vibrational frequencies of NO_3 are challenging to compute accurately, we used the observed vibrational frequencies as tabulated in the MultiWell Thermodynamics Database (Barker et al., 2017) rather than the computed values. Using the calculated vibrational frequencies lowered K_c modestly, by 9% to 16% for 200 K ≤ T ≤ 320 K. Using the vibrational energy levels of Viel and Eisfeld (2018) raised K_c by 2.4% at 200 K and lowered K_c by 4.2%, with a monotonic progression between those two temperatures. These uncertainties in K_c are much smaller than those due to the uncertainty in D_0, which creates a factor of 5 uncertainty at 298 K). As we show below, this uncertainty will not change the conclusions of our analysis of the experiments of Sommar et al. (1997) or the field study of Peleg et al. (2015).

Table 1. Temperature dependence of the equilibrium constant (K_c, cm^3 $molecule^{-1}$) for reaction (2) based on SFX2C-1e-EOMIP-CCSDT/ANORCC1 for energies, CCSD/ANORCC1 for rotational constants, and experimental values of vibrational frequencies.

T (K)	K_c
200	1.5×10^{-17}
220	3.3×10^{-18}
240	9.6×10^{-19}
260	3.3×10^{-19}
280	1.3×10^{-19}
298.15	6.5×10^{-20}
300	6.1×10^{-20}
320	3.1×10^{-20}

3.2 Bimolecular reactions of NO_3Hg radical

We investigated the reactions of $NO_3Hg^{(I)}$• with ozone and with some of the more abundant radicals in the atmosphere: Z = O_2, NO_2, HOO, NO_3, and BrO. To help analyze the experimental work of Sommar et al. (1997) we also studied the reactions of $NO_3Hg^{(I)}$• with NO_3 and HNO_3.

As can be seen from Fig.2, $NO_3Hg^{(II)}$-Z bond energies are only slightly lower than those for $HOHg^{(II)}$-Z; we previously showed the near-equivalence of $HOHg^{(II)}$-Z and $BrHg^{(II)}$-Z bond energies (see Dibble et al., 2020). For $NO_3Hg^{(II)}$-NO_3, for which no $HOHg^{(II)}NO_3$ or $BrHg^{(II)}NO_3$ analogues appear in the literature, the bond energy is 64.4 kcal mol^{-1}. All bond energies are tabulated in the Supporting Information (Table S7). We verified that these radical-radical addition reactions proceed without a barrier, except in the cases of Z = O_2 and NO_3. Note that previous calculations established the presence of a barrier to $BrHg^{(I)}$• + O_2 + M → $BrHg^{(II)}OO$ + M (Wu et al., 2022).

Reaction of $NO_3Hg^{(I)}$• with ozone to produce $NO_3Hg^{(II)}O$ + O_2 is significantly exothermic ($\Delta H_r^\circ(0\ K)$ = -46.3 kcal mol^{-1}) and possesses no barrier. This suggests that the rate constant for this reaction may be as high as that for $BrHg^{(I)}$• + O_3 (7.5×10^{-11}

cm^3 molecule^{-1} sec^{-1} at room temperature) (Castro et al., 2022; Gómez Martín et al., 2022). This suggests that the major bimolecular reaction of $NO_3Hg^{(I)}$• in the atmosphere, like $HOHg^{(I)}$• and $BrHg^{(I)}$•, is reaction with ozone (Shah et al., 2021).

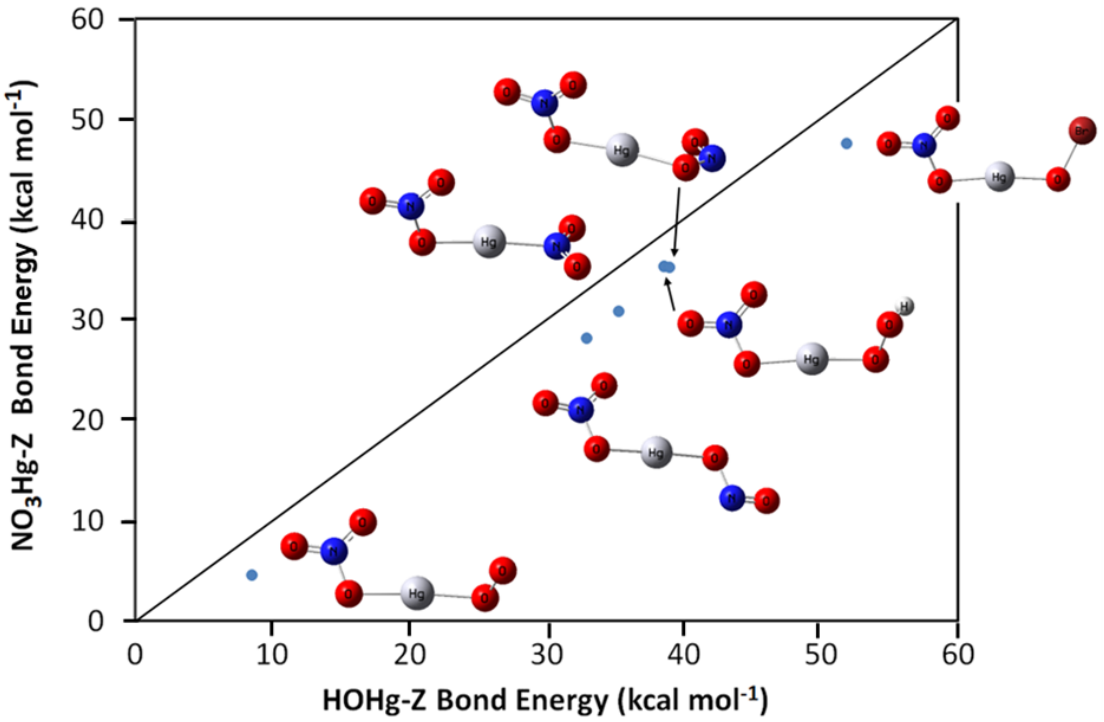

Figure 2. Bond energies (ZPE-corrected) at 0 K for $NO_3Hg^{(II)}$-Z versus $HOHg^{(II)}$-Z for Z = O_2, NO_2, HOO, and BrO at PBE0/AVTZ. Note that D_0 has not been reported for either HOHg-NO_3 or BrHg-NO_3, so $Hg(NO_3)_2$ (D_0 = 64.4 kcal mol^{-1}) is not included in this Figure.

Reinterpreting the Experimental Study of k($Hg^{(0)}$ + NO_3)

Sommar et al. (1997) used a fast-flow discharge reactor to investigate the rate constant for $Hg^{(0)}$ + NO_3 at total pressures of 5.4 – 9.4 hPa in He. Based on previous work using the same reactor at similar pressures, the flow velocity in the reactor probably exceeded 100 cm sec^{-1} (Langer et al., 1993). Given the total reactor length of 1 meter, the reaction time would be less than one second. Nitrate radical was produced from F + HNO_3 before Hg entered the reactor, and was initially present (8-17 × 10^{12} molecule cm^{-3}) in excess over $Hg^{(0)}$ (0.7-2.1 × 10^{12} molecule cm^{-3}). Sommar et al. (1997) assumed that reaction of NO_3 with $Hg^{(0)}$ was irreversible on the time scale of the experiment. This assumption was not unreasonable given the erroneous data then available on ΔH_f^0 for HgO (Grade and Hirschwald, 1982), from which it was assumed that the following reaction was thermodynamically favorable:

$$Hg^{(0)} + NO_3 \rightarrow Hg^{(II)}O + NO_2 \quad (7)$$

However, three quantum chemical studies using three different approaches show that $Hg^{(II)}O$ is very weakly bound (3-6 kcal mol^{-1}) (Filatov and Cremer, 2004; Peterson et al., 2007; Shepler and Peterson, 2003), which renders reaction (7) so endothermic ($\Delta H_r^\circ \approx +45$ kcal mol^{-1}) that it will not occur. We view $NO_3Hg^{(I)}$• as the only reasonable product of reaction of NO_3 with $Hg^{(0)}$. If $NO_3Hg^{(I)}$• falls apart to regenerate $Hg^{(0)}$ faster than, or in competition with, its reaction to form $Hg^{(II)}$, then the upper limit reported by Sommar et al. would not be valid. Therefore, we next consider whether bimolecular reactions of $NO_3Hg^{(I)}$• could compete with dissociation of $NO_3Hg^{(I)}$• to $NO_3 + Hg^{(0)}$ under the experimental conditions of Sommar et al. (1997).

Oxidation of $NO_3Hg^{(I)}$• to $Hg^{(II)}$ could occur via reaction with HNO_3:

$$NO_3Hg^{(I)}\bullet + HNO_3 \rightarrow NO_3Hg^{(II)}H + NO_3 \quad (8a)$$

$$NO_3Hg^{(I)}\bullet + HNO_3 \rightarrow Hg^{(II)}(NO_3)_2 + H \quad (8b)$$

We find these reactions to be significantly endothermic (at CAM-B3LYP-D3BJ/AVTZ). $\Delta H_r^0(0\ K)$ is +24 kcal mol^{-1} for (8a) and +39 kcal mol^{-1} for (8b). We estimate an upper limit to the rate constant for the less endothermic reaction channel (8a). The estimate is made via $k_{8a}(T) = Ae^{-E_a/RT}$, taking $\Delta H_r^0(0\ K)$ as a lower limit for E_a and 10^{-10} cm^3 $molecule^{-1}$ sec^{-1} as the upper limit to A. This approximation gives $k_{8a}(298) < 10^{-26}$ cm^3 $molecule^{-1}$ sec^{-1}. But even if we assume that the DFT value of $\Delta H_r^0(0\ K)$ exceeds the true value by as much as 10 kcal mol^{-1}, we get $k_{8a}(298) < 10^{-20}$ cm^3 $molecule^{-1}$ sec^{-1}. The HNO_3 concentration was not given, but must have been a modest fraction of the total pressure of 5.4-9.4 hPa (9.8×10^{17} molecule cm^{-3}). Using the upper limit to k_{8b}, and $[HNO_3] = 1$ hPa, the pseudo-first order rate constant ($k_{8a}' = k_{8a}[HNO_3]$) for $HgNO_3$ loss falls below 10^{-2} sec^{-1}, corresponding to a lifetime greater than 100 sec. Clearly, HNO_3 did not contribute to gas-phase loss of $HgNO_3$ in the available reaction time of 1 second.

As discussed above, $NO_3Hg^{(I)}$• can react with NO_3 over a barrier to make $Hg^{(II)}(NO_3)_2$:

$$NO_3Hg^{(I)}\bullet + NO_3 \rightarrow Hg^{(II)}(NO_3)_2 \quad (9)$$

We simulated the gas-phase formation and dissociation of $NO_3Hg^{(I)}$• (reactions 2 and -2) along with reaction (9) in Kintecus (Ianni, 2003, 2019) over 1 second, equal to our estimate of the longest reaction time in the experiment. We set k_9 at 10^{-10} cm^3 $molecule^{-1}$ s^{-1} to maximize the formation of Hg(II). We varied k_2 between 10^{-10} and 10^{-16} cm^3 $molecule^{-1}$ s^{-1} and computed k_{-2} from K_c at 298 K (see Table 1). For $k_2 > 5 \times 10^{-15}$ cm^3 $molecule^{-1}$ s^{-1}, the concentration of $NO_3Hg^{(I)}$• was controlled by equilbrium to within 1%, and the loss of GEM was less than 0.2% at 1 second. Figure 3 depicts the time evolution of $[Hg^{(0)}]$, $[NO_3Hg^{(I)}\bullet]$, and $[Hg^{(II)}(NO_3)_2]$ under these conditions. The small fractional losses of GEM in our simulations would not have been observable by Sommar et al. against the wall loss that dominated their experiment. Even if K_c was ten times higher than computed here, the simulated gas-phase loss of GEM could not have exceeded 1.4%, amounting to less than 3% of the loss of GEM to the walls at their lower S/V ratio for a one-second reaction time. Given that reported 20% uncertainty in the effective second-order rate constant for wall loss under these conditions, this small extent of gas-phase loss would not have been noticeable. Therefore, the work of Sommar et al. (1997) does not constrain the value of k_2.

In separate experiments, Sumner et al. (2005) briefly reported on upper limits to k_2 of 7-30 × 10^{-15} cm^3 $molecule^{-1}$ s^{-1} in chamber experiments in 1 atm of air. They did not report any concentration data that would allow us to simulate the conditions of their experiment. Given that k_2 is expected to be pressure-dependent, its value at this pressure would probably greatly exceed its value under the conditions of Sommar et al. (in 5-10 kPa of He).

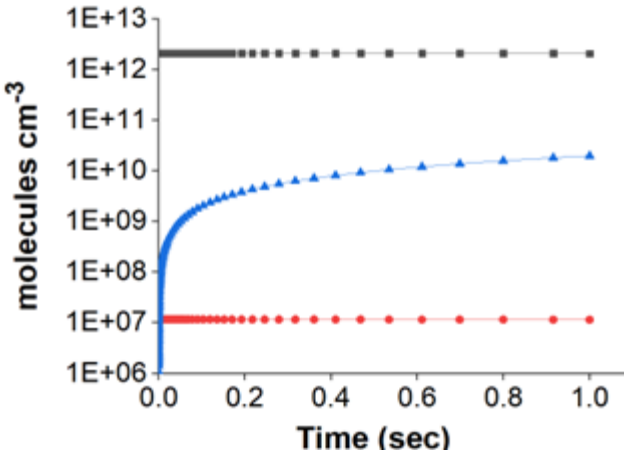

Figure 3. Simulated time evolution of [Hg] (■), [$NO_3Hg^{(I)}$•] (●), and [$Hg^{(II)}(NO_3)_2$] (▲) in the experiment of Sommar et al., (1997)**. This simulation used [$Hg^{(0)}]_0$ = 2.1 × 10^{13} molecule cm^{-3} and [$NO_3]_0$ = 1.7 × 10^{13} molecule cm^{-3}, which were the highest concentrations used in the experiment.**

3.4 NO_3-Initiated Oxidation of GEM Cannot Explain Nighttime GOM Production in Peleg et al.

Peleg et al. (2015) reported strong correlations between nighttime [GOM] and [NO_3] over their six-week study period, but an absence of correlation with [GEM], [particulate mercury], [O_3], [CO], [SO_2], [sulfate], or wind direction. Citing the argument of (Dibble et al. (2012) that the instability of $NO_3Hg^{(I)}$• would prevent it from initiating oxidation of GEM, Peleg et al. were careful to suggest that NO_3 was "involved" in GEM oxidation, rather than initiating GEM oxidation. However, we know of only two roles for oxidants in $Hg^{(II)}$ production: either initiation by forming $Hg^{(I)}$ or oxidation of $Hg^{(I)}$ to $Hg^{(II)}$. Subsequent to the publication of Peleg, et al., it was learned that ozone can oxidize $Hg^{(I)}$ to $Hg^{(II)}$ with a high rate constant (k_5 = 7.5 ×10^{-11} cm^3 $molecule^{-1}$ s^{-1}) (Castro et al., 2022; Gómez Martín et al., 2022). Given this high rate constant, the 69 ± 75 ng m^{-3} of NO_3 present under the conditions of Peleg et al. would not measurably increase the rate of oxidation of $Hg^{(I)}$ over that caused by 90 ± 28 μg m^{-3} of ozone. However, the discovery of the reaction of $Hg^{(I)}$ with ozone could revise our estimates of the potential role of weakly-bound Hg(I) species in GEM oxidation. Consider, for example, initiation by OH radical: OH had been thought to contribute < 1% to global GEM oxidation (Dibble et al., 2020), but adding to models the reaction $HOHg^{(I)}$• + O_3 → $HOHg^{(II)}O$ • + O_3 increases the global influence of OH to ~30% (Shah et al., 2021). More recently, Lee et al. (2024) suggested that atomic iodine can initiate oxidation despite the low bond energy of $IHg^{(I)}$(Cremer et al., 2008; Salter et al., 1986; Shepler

et al., 2005). Accordingly, to investigate the role of NO_3 in oxidation of GEM to GOM, we simulated the potential for nitrate radical to initiate production of GOM with the following mechanism:

$$Hg + NO_3 + M \leftrightarrows NO_3Hg^{(I)}\bullet + M \qquad (R_2, R_{-2})$$

$$NO_3Hg^{(I)}\bullet + O_3 \rightarrow NO_3Hg^{(II)}O\bullet + O_2 \qquad (R_{10})$$

Our mechanism omits the subsequent reactions of $NO_3Hg^{(II)}O\bullet$. By analogy to $HOHg^{(II)}O\bullet$ and $BrHg^{(II)}O\bullet$, we presume that reactions of $NO_3Hg^{(II)}O\bullet$ with volatile organic compounds (VOCs) and NO_x would lead to formation of closed-shell GOM compounds (Hewa Edirappulige et al., 2023; Lam et al., 2019a, b). But reaction of $NO_3Hg^{(II)}O\bullet$ with CO would yield $NO_3Hg^{(I)}\bullet$ (Hewa Edirappulige et al., 2023; Khiri et al., 2019) thereby reducing [GOM] below the total $[NO_3Hg^{(II)}O\bullet]$ produced. We cannot address these competing processes due to the absence of concentration data for the study site, as well as the absence of information on the rate constants for these reactions. As a result, we report the *total production* of GOM, which would exceed the resulting *concentrations* of GOM.

We selected simulation conditions and rate constants that bias our simulations towards high production of GOM. Specifically, we used the highest values of reactant concentrations reported by Peleg et al.: $[Hg^{(0)}] = 2.6$ ng m^{-3} (7.8×10^6 molecule cm^{-3}), $[NO_3] = 430$ ng m^{-3} (4.2×10^9 molecule cm^{-3}), and $[O_3] = 200$ µg m^{-3} (2.1×10^{12} molecule cm^{-3}). We also simulated 12 hours of reaction time for these summer nights. Despite these choices biasing the simulation to *over*estimate GOM production, GOM production over 12 hours was only 1.8×10^4 molecule cm^{-3} (6.0 pg m^{-3}), which is much less than the average *observed* [GOM] of 24 pg m^{-3}, let alone the peak values of > 90 pg m^{-3}. Note that the rate of GOM production in this case is proportional to $[GEM] \times [NO_3] \times [O_3]$; by using the maximum concentrations of all three species, we artificially overestimate GOM production by a factor of 20 relative to the obsevations. Furthermore, the simulations held [GEM], $[NO_3]$, and $[O_3]$ constant, whereas Peleg et al., (2015) reported concentrations varying considerably during a single night. In addition, we used $k_2 = k_{10} = 10^{-10}$ cm^3 molecule^{-1} s^{-1}, that is, near the collision limit. This value may not be unreasonable for k_{10} (Castro et al., 2022; Gómez Martín et al., 2022), but it exceeds the rate constants for the analogous reactions forming BrHg (Donohoue et al., 2006) and HOHg (Pal and Ariya, 2004; Sommar et al., 2001) by factors of ~300 and ~1000, respectively (at 1 atm near 298 K). Given all these factors the factor of 5 uncertainty in K_c cannot have caused the discrepancy between our results and the observations of Peleg et al., (2015). Finally, the KCl denuder used to trap GOM is now known to underestimate the true concentriaton of GOM by a factor of two to four (Dunham-Cheatham et al., 2023; Gustin et al., 2024) So the true [GOM] was likely much higher than that reported.

As a result, we conclude that gas-phase reaction of NO_3 with GEM contributed very little to formation of the GOM observed by Peleg et al (2015). One might invoke surface reactions to explain their observations, especially considering that surface reactions dominated the loss of GEM in the experiment of Sommar, et al (1997). However, the surface-to-volume ratios of 2.7 cm^{-1} and 1.3 cm^{-1} in their experiments greatly exceeds those in aerosols or the outdoor environment. Recalling our arguments,

above, that NO_3 could not have measurably increased the rate of $Hg^{(I)}$ oxidation to gaseous $Hg^{(II)}$, it is hard to see how NO_3 could have played any appreciable role in generating the GOM observed by Peleg et al.

4. Conclusions

We find the NO_3-Hg bond energy, D_0, to be only 6.5 kcal mol^{-1}, leading to an equilibrium constant of only 6.5×10^{-20} cm^3 $molecule^{-1}$ at 298 K. While this bond energy is slightly higher than that previously calculated, it so low that $NO_3Hg^{(I)}$• is likely to fall apart very rapidly. Our kinetic analysis demonstrates that gas phase oxidation of $Hg^{(0)}$ initiated by nitrate radical was too slow to contribute significantly to loss of Hg(0) in the experiment of Sommar et al. (1997) or the field study of Peleg et al. (2015). This holds true even if we assume that association of NO_3 with $Hg^{(0)}$ occurs with a rate constant comparable to the collision limit. This means that one cannot rely on the upper limit reported by Sommar et al. (1997). The fact that $[O_3] \approx 1000$ $[NO_3]$ in the field work of Peleg et al. (2015), along with the barrier to association of $NO_3Hg^{(I)}$• with NO_3, means that NO_3 cannot have significantly increased the rate of oxidation of $NO_3Hg^{(I)}$• to GOM. Consequently, the correlation between $[NO_3]$ and [GOM] found by Peleg et al. (2015) did not result from the involvement of nitrate radicals in nighttime oxidation of mercury.

Given that $[O_3]$ usually greatly exceeds the summed concentration of radicals in the atmosphere, we conclude one can reasonably approximate the rate of oxidation of $NO_3Hg^{(I)}$• to Hg(II) as being proportional to $k_{10}[O_3]$. Given the low equilibrium constant for formation of $NO_3Hg^{(I)}$•, it would require very high $[O_3] \times [NO_3]$ for NO_3 to initiate significant gas-phase oxidation of GEM to GOM near 298 K. Our results do not rule out the participation of NO_3 in initiating oxidation of GEM to GOM under the colder conditions of the middle and upper troposphere. The potential impact of this oxidation route on mercury redox chemistry in the global atmosphere is difficult to assess without carrying out a global modeling study, which is beyond the scope of this paper.

Author Contributions. TSD conceived the project. DTHE, LC, and PJC carried out quantum calculations. DTHE and LC wrote the original draft. DTHE and TSD carried and kinetic simulations. All authors reviewed and edited the manuscript.

Competing interests. The authors declare that they have no conflicts of interest.

Financial Support. Work at SUNY-ESF (DHTE, PJC, & TSD) was supported by the National Science Foundation under Grant 2004100. Work at the Johns Hopkins University (LC) has been supported by the Department of Energy, Office of Science, Office of Basic Energy Sciences under Award Number DE-SC0020317.

References

Adamo, C. and Barone, V.: Toward reliable density functional methods without adjustable parameters: The PBE0 model, J Chem Phys, 110, 6158–6170, https://doi.org/10.1063/1.478522, 1999.

Asthana, A., Liu, J., and Cheng, L.: Exact two-component equation-of-motion coupled-cluster singles and doubles method using atomic mean-field spin-orbit integrals, J Chem Phys, 150, 074102, https://doi.org/10.1063/1.5081715, 2019.

Barker, J. R.: Multiple-Well, multiple-path unimolecular reaction systems. I. MultiWell computer program suite, Int J Chem Kinet, 33, 232–245, https://doi.org/10.1002/kin.1017, 2001.

Barker, J. R.: Energy transfer in master equation simulations: A new approach, Int J Chem Kinet, 41, 748–763, https://doi.org/10.1002/kin.20447, 2009.

Barker, J. R., Nguyen, T. L., Stanton, J. F., Aieta, C., Ceotto, M., Gabas, F., Kumar, T. J. D., Li, C. G. L., Lohr, L. L., Maranzana, A., Ortiz, N. F., Preses, J. M., Simmie, J. M., Sonk, J. A., and Stimac, P. J.: MultiWell Thermodynamic Database, Ann Arbor, MI, 2017.

Barker, J. R., Nguyen, T. L., Stanton, J. F., Aieta, C., Ceotto, M., Gabas, F., Kumar, T. J. D., Li, C. G. L., Lohr, L. L., Maranzana, A., Ortiz, N. F., Preses, J. M., Simmie, J. M., Sonk, J. A., and Stimac, P. J.: MultiWell-2023 Software Suite, 2023.

Brown, S. S. and Stutz, J.: Nighttime radical observations and chemistry, Chem Soc Rev, 41, 6405, https://doi.org/10.1039/c2cs35181a, 2012.

Castro, P. J., Kellö, V., Cernušák, I., and Dibble, T. S.: Together, Not Separately, OH and O3 Oxidize Hg(0) to Hg(II) in the Atmosphere, J Phys Chem A, 126, 8266–8279, https://doi.org/10.1021/acs.jpca.2c04364, 2022.

Cheng, L. and Gauss, J.: Analytic energy gradients for the spin-free exact two-component theory using an exact block diagonalization for the one-electron Dirac Hamiltonian, J Chem Phys, 135, https://doi.org/10.1063/1.3624397, 2011.

Chua, G., Naik, V., and Horowitz, L. W.: Exploring the drivers of tropospheric hydroxyl radical trends in the Geophysical Fluid Dynamics Laboratory AM4.1 atmospheric chemistry–climate model, Atmos Chem Phys, 23, 4955–4975, https://doi.org/10.5194/acp-23-4955-2023, 2023.

Cremer, D., Kraka, E., and Filatov, M.: Bonding in mercury molecules described by the normalized elimination of the small component and coupled cluster theory., Chemphyschem, 9, 2510–21, https://doi.org/10.1002/cphc.200800510, 2008.

Dibble, T. S., Zelie, M. J., and Mao, H.: Thermodynamics of reactions of ClHg and BrHg radicals with atmospherically abundant free radicals, Atmos Chem Phys, 12, 10271–10279, https://doi.org/10.5194/acp-12-10271-2012, 2012.

Dibble, T. S., Zelie, M. J., and Mao, H.: Erratum: Thermodynamics of reactions of ClHg and BrHg radicals with atmospherically abundant free radicals (Atmospheric Chemistry and Physics (2012) 12 (10271-10279)), Atmos Chem Phys, 13, https://doi.org/10.5194/acp-13-9211-2013, 2013.

Dibble, T. S., Tetu, H. L., Jiao, Y., Thackray, C. P., and Jacob, D. J.: Modeling the OH-Initiated Oxidation of Mercury in the Global Atmosphere without Violating Physical Laws, J Phys Chem A, 124, 444–453, https://doi.org/10.1021/acs.jpca.9b10121, 2020.

Dixon, D. A., Peterson, K. A., and Francisco, J. S.: The Molecular Structures and Energetics of Cl_2 CO, ClCO, Br_2 CO, and BrCO, J Phys Chem A, 104, 6227–6232, https://doi.org/10.1021/jp0005571, 2000.

Donohoue, D. L., Bauer, D., Cossairt, B., and Hynes, A. J.: Temperature and Pressure Dependent Rate Coefficients for the Reaction of Hg with Br and the Reaction of Br with Br: A Pulsed Laser Photolysis-Pulsed Laser Induced Fluorescence Study, Journal of Physical Chemistry A, 110, 6623–6632, https://doi.org/10.1021/JP054688J, 2006.

Dunham-Cheatham, S. M., Lyman, S., and Gustin, M. S.: Comparison and calibration of methods for ambient reactive mercury quantification, Science of The Total Environment, 856, 159219, https://doi.org/10.1016/j.scitotenv.2022.159219, 2023.

Dunning, T. H.: Gaussian basis sets for use in correlated molecular calculations. I. The atoms boron through neon and hydrogen, J Chem Phys, 90, 1007–1023, https://doi.org/10.1063/1.456153, 1989.

Dyall, K. G.: Interfacing relativistic and nonrelativistic methods. IV. One- and two-electron scalar approximations, J Chem Phys, 115, 9136–9143, https://doi.org/10.1063/1.1413512, 2001.

Eisfeld, W. and Morokuma, K.: A detailed study on the symmetry breaking and its effect on the potential surface of NO3, J Chem Phys, 113, 5587–5597, https://doi.org/10.1063/1.1290607, 2000.

Faegri Jr, K.: Relativistic Gaussian basis sets for the elements K - Uuo, Theor Chem Acc, 105, 252–258, https://doi.org/10.1007/s002140000209, 2001.

Figgen, D., Rauhut, G., Dolg, M., and Stoll, H.: Energy-consistent pseudopotentials for group 11 and 12 atoms: adjustment to multi-configuration Dirac–Hartree–Fock data, Chem Phys, 311, 227–244, https://doi.org/10.1016/j.chemphys.2004.10.005, 2005.

Filatov, M. and Cremer, D.: Revision of the dissociation energies of mercury chalcogenides--unusual types of mercury bonding., Chemphyschem, 5, 1547–57, https://doi.org/10.1002/cphc.200301207, 2004.

Frisch, M. J., Trucks, G. W., Schlegel, H. B., Scuseria, G. E., Robb, M. A., Cheeseman, J. R., Scalmani, G., Barone, V., Petersson, G. A., Nakatsuji, H., Li, X., Caricato, M., Marenich, A. V., Bloino, J., Janesko, B. G., Gomperts, R., Mennucci, B., Hratchian, D. J., Ortiz, J. V., Izmaylov, A. O., Sonnenberg, J. L., Williams-Young, D., Ding, F., Lipparini, F., Egidi, F., Goings, J., Peng, B., Petrone, A., Henderson, T., Ranasinghe, D., Zakrzewski, V. G., Gao, J., Rega, N., Zheng, G., Liang, W., Hada, M., Ehara, M., Toyota, K., Fukuda, R., Hasegawa, J., Ishida, M., Nakajima, T., Honda, Y., Kitao, O., Nakai, H., Vreven, T., Throssell, K., Montgomery, Jr. , J. A., Peralta, J. E., Ogliaro, F., Bearpark, M. J., Heyd, J. J., Brothers, E. N., Kudin, K. N., Staroverov, V. N., Keith, T. A., Kobayashi, R., Normand, J., Raghavachari, K., Rendell, A. P., Burant, J. C., Iyengar, S. S., Tomasi, J., Cossi, M. M., Millam, J. M., Klene, M., Adamo, C., Cammi, R., Ochterski, J. W., Martin, R. L., Morokuma, K., Farkas, O., Foresman, J. B., and Fox, D. J.: Gaussian 16, Rev. A, 2016.

Gómez Martín, J. C., Lewis, T. R., Douglas, K. M., Blitz, M. A., Saiz-Lopez, A., and Plane, J. M. C.: The reaction between HgBr and O_3: kinetic study and atmospheric implications, Physical Chemistry Chemical Physics, 24, 12419–12432, https://doi.org/10.1039/D2CP00754A, 2022.

Goodsite, M. E. Plane, J. M. C. and Skov, H.: A Theoretical Study of the Oxidation of Hg^0 to $HgBr_2$ in the Troposphere, Environ. Sci. Technol., 38, 1772–1776, https://doi.org/10.1021/es034680s, 2004.

Grade, M. and Hirschwald, W.: Energetics and Stabilities of the IIB/VIA-Compounds at High-Temperature Equilibrium Conditions, Berichte der Bunsengesellschaft für physikalische Chemie, 86, 899–907, https://doi.org/10.1002/bbpc.19820861006, 1982.

Grimme, S., Ehrlich, S., and Goerigk, L.: Effect of the damping function in dispersion corrected density functional theory, J Comput Chem, 32, 1456–1465, https://doi.org/10.1002/jcc.21759, 2011.

Gustin, M. S., Dunham-Cheatham, S. M., Lyman, S., Horvat, M., Gay, D. A., Gačnik, J., Gratz, L., Kempkes, G., Khalizov, A., Lin, C.-J., Lindberg, S. E., Lown, L., Martin, L., Mason, R. P., MacSween, K., Vijayakumaran Nair, S., Nguyen, L. S. P., O'Neil, T., Sommar, J., Weiss-Penzias, P., Zhang, L., and Živković, I.: Measurement of Atmospheric Mercury: Current Limitations and Suggestions for Paths Forward, Environ Sci Technol, 58, 12853–12864, https://doi.org/10.1021/acs.est.4c06011, 2024.

Helgaker, T., Klopper, W., Koch, H., and Noga, J.: Basis-set convergence of correlated calculations on water, J Chem Phys, 106, 9639–9646, https://doi.org/10.1063/1.473863, 1997.

Heß, B. A., Marian, C. M., Wahlgren, U., and Gropen, O.: A mean-field spin-orbit method applicable to correlated wavefunctions, Chem Phys Lett, 251, 365–371, https://doi.org/10.1016/0009-2614(96)00119-4, 1996.

Hewa Edirappulige, D. T., Kirby, I. J., Beckett, C. K., and Dibble, T. S.: Atmospheric Chemistry of HOHg(II)O• Mimics That of a Hydroxyl Radical, J Phys Chem A, 127, 8392–8403, https://doi.org/10.1021/acs.jpca.3c04159, 2023.

Horowitz, H. M., Jacob, D. J., Zhang, Y., Dibble, T. S., Slemr, F., Amos, H. M., Schmidt, J. A., Corbitt, E. S., Marais, E. A., and Sunderland, E. M.: A new mechanism for atmospheric mercury redox chemistry: implications for the global mercury budget, Atmos. Chem. Phys., 17, 6353–6371, https://doi.org/10.5194/acp-17-6353-2017, 2017.

Hynes, A. J., Donohoue, D. L., Goodsite, M. E., and Hedgecock, I. M.: Our current understanding of major chemical and physical processes affecting mercury dynamics in the atmosphere and at the air-water/terrestrial interfaces, in: Mercury Fate and Transport in the Global Atmosphere: Emissions, Measurements and Models, Springer US, 427–457, https://doi.org/10.1007/978-0-387-93958-2_14, 2009.

Ianni, J. C.: A comparison of the Bader-Deuflhard and the Cash-Karp Runge-Kutta integrators for the GRI-MECH 3.0 model based on the chemical kinetics code Kintecus, in: Computational Fluid and Solid Mechanics 2003, Elsevier, 1368–1372, https://doi.org/10.1016/B978-008044046-0.50335-3, 2003.

Ianni, J. C.: Kintecus, www.kintecus.com., 2019.

Jiao, Y. and Dibble, T. S.: Quality Structures, Vibrational Frequencies, and Thermochemistry of the Products of Reaction of BrHg with NO_2, HO_2, ClO, BrO, and IO, J Phys Chem A, 119, 10502–10510, https://doi.org/10.1021/acs.jpca.5b04889, 2015.

Kendall, R. A., Dunning, T. H., and Harrison, R. J.: Electron affinities of the first-row atoms revisited. Systematic basis sets and wave functions, J Chem Phys, 96, 6796–6806, https://doi.org/10.1063/1.462569, 1992.

Khan, M. A. H., Cooke, M. C., Utembe, S. R., Archibald, A. T., Derwent, R. G., Xiao, P., Percival, C. J., Jenkin, M. E., Morris, W. C., and Shallcross, D. E.: Global modeling of the nitrate radical (NO_3) for present and pre-industrial scenarios, Atmos Res, 164–165, 347–357, https://doi.org/10.1016/j.atmosres.2015.06.006, 2015.

Khiri, D., Louis, F., Cernusak, I., and Dibble, T.: BrHgO˙ + CO: Analogue of OH + CO and Reduction Path for Hg(II) in the Atmosphere, ACS Earth Space Chem, 4, 1777–1784, https://doi.org/10.1021/acsearthspacechem.0c00171, 2019.

Kutzelnigg, W. and Liu, W.: Quasirelativistic theory equivalent to fully relativistic theory, J Chem Phys, 123, https://doi.org/10.1063/1.2137315, 2005.

Lam, K. T., Wilhelmsen, C. J., and Dibble, T. S.: BrHgO• + C_2H_4 and BrHgO• + HCHO in Atmospheric Oxidation of Mercury: Determining Rate Constants of Reactions with Pre-Reactive Complexes and a Bifurcation, J Phys Chem A, 123, 6045–6055, https://doi.org/10.1021/acs.jpca.9b05120, 2019a.

Lam, K. T., Wilhelmsen, C. J., Schwid, A. C., Jiao, Y., and Dibble, T. S.: Computational Study on the Photolysis of BrHgONO and the Reactions of BrHgO• with CH_4, C_2H_6, NO, and NO_2: Implications for Formation of Hg(II) Compounds in the Atmosphere, J Phys Chem A, 123, 1637–1647, https://doi.org/10.1021/acs.jpca.8b11216, 2019b.

Langer, S., Ljungström, E., and Wängberg, I.: Rates of reaction between the nitrate radical and some aliphatic esters, J. Chem. Soc., Faraday Trans., 89, 425–431, https://doi.org/10.1039/FT9938900425, 1993.

Lee, C. F., Elgiar, T., David, L. M., Wilmot, T. Y., Reza, M., Hirshorn, N., McCubbin, I. B., Shah, V., Lin, J. C., Lyman, S. N., Hallar, A. G., Gratz, L. E., and Volkamer, R.: Elevated Tropospheric Iodine Over the Central Continental United States: Is Iodine a Major Oxidant of Atmospheric Mercury?, Geophys Res Lett, 51, https://doi.org/10.1029/2024GL109247, 2024.

Liu, J. and Cheng, L.: An atomic mean-field spin-orbit approach within exact two-component theory for a non-perturbative treatment of spin-orbit coupling, J Chem Phys, 148, https://doi.org/10.1063/1.5023750, 2018.

Liu, W. and Peng, D.: Exact two-component Hamiltonians revisited, J Chem Phys, 131, https://doi.org/10.1063/1.3159445, 2009.

Mao, H., Talbot, R. W., Sigler, J. M., Sive, B. C., and Hegarty, J. D.: Seasonal and diurnal variations of Hg° over New England, Atmos Chem Phys, 8, 1403–1421, https://doi.org/10.5194/acp-8-1403-2008, 2008.

Matthews, D. A. and Stanton, J. F.: Non-orthogonal spin-adaptation of coupled cluster methods: A new implementation of methods including quadruple excitations, J Chem Phys, 142, https://doi.org/10.1063/1.4907278, 2015.

Matthews, D. A., Cheng, L., Harding, M. E., Lipparini, F., Stopkowicz, S., Jagau, T.-C., Szalay, P. G., Gauss, J., and Stanton, J. F.: Coupled-cluster techniques for computational chemistry: The CFOUR program package, J. Chem. Phys., 152, 214108, https://doi.org/10.1063/5.0004837, 2020.

Mills, I. M.: Modern Spectroscopy: Modern Research, edited by: Rao, K. and Mathews, C., Academic Press, NewYork, 115–140 pp., 1972.

Neese, F.: The ORCA program system, WIREs Computational Molecular Science, 2, 73–78, https://doi.org/10.1002/wcms.81, 2012.

Neese, F.: Software update: The *ORCA* program system—Version 5.0, WIREs Computational Molecular Science, 12, https://doi.org/10.1002/wcms.1606, 2022.

Pal, B. and Ariya, P. A.: Gas-phase HO-initiated reactions of elemental mercury: kinetics, product studies, and atmospheric implications., Environ Sci Technol, 38, 5555–5566, 2004.

Peleg, M., Tas, E., Obrist, D., Matveev, V., Moore, C., Gabay, M., and Luria, M.: Observational Evidence for Involvement of Nitrate Radicals in Nighttime Oxidation of Mercury, Environ Sci Technol, 49, 14008–14018, https://doi.org/10.1021/acs.est.5b03894, 2015.

Penkett, S. A., Burgess, R. A., Coe, H., Coll, I., Hov, Ø., Lindskog, A., Schmidbauer, N., Solberg, S., Roemer, M., Thijsse, T., Beck, J., and Reeves, C. E.: Evidence for large average concentrations of the nitrate radical (NO_3) in Western Europe from the HANSA hydrocarbon database, Atmos Environ, 41, 3465–3478, https://doi.org/10.1016/j.atmosenv.2006.11.055, 2007.

Peterson, K. A. and Dunning, T. H.: Accurate correlation consistent basis sets for molecular core-valence correlation effects: The second row atoms Al-Ar, and the first row atoms B-Ne revisited, J Chem Phys, 117, 10548–10560, https://doi.org/10.1063/1.1520138, 2002.

Peterson, K. A. and Puzzarini, C.: Systematically convergent basis sets for transition metals. II. Pseudopotential-based correlation consistent basis sets for the group 11 (Cu, Ag, Au) and 12 (Zn, Cd, Hg) elements, Theor Chem Acc, 114, 283–296, https://doi.org/10.1007/s00214-005-0681-9, 2005.

Peterson, K. A., Figgen, D., Goll, E., Stoll, H., and Dolg, M.: Systematically convergent basis sets with relativistic pseudopotentials. II. Small-core pseudopotentials and correlation consistent basis sets for the post-d group 16–18 elements, J Chem Phys, 119, 11113, https://doi.org/10.1063/1.1622924, 2003.

Peterson, K. A., Shepler, B. C., and Singleton, J. M.: The group 12 metal chalcogenides: an accurate multireference configuration interaction and coupled cluster study, Mol Phys, 105, 1139–1155, https://doi.org/10.1080/00268970701241664, 2007.

Roos, B. O., Malmqvist, P.-Å., Veryazov, V., and Widmark, P.-O.: Main Group Atoms and Dimers Studied with a New Relativistic ANO Basis Set, J Phys Chem A, 108, 2851–2858, 2003.

Roos, B. O., Lindh, R., Malmqvist, P.-Å., Veryazov, V., and Widmark, P.-O.: New Relativistic ANO Basis Sets for Transition Metal Atoms, J Phys Chem A, 109, 6575–6579, https://doi.org/10.1021/JP0581126, 2005.

Rosanka, S., Vu, G. H. T., Nguyen, H. M. T., Pham, T. V., Javed, U., Taraborrelli, D., and Vereecken, L.: Atmospheric chemical loss processes of isocyanic acid (HNCO): a combined theoretical kinetic and global modelling study, Atmos Chem Phys, 20, 6671–6686, https://doi.org/10.5194/acp-20-6671-2020, 2020.

Saiz-Lopez, A., Sitkiewicz, S. P., Roca-Sanjuán, D., Oliva-Enrich, J. M., Dávalos, J. Z., Notario, R., Jiskra, M., Xu, Y., Wang, F., Thackray, C. P., Sunderland, E. M., Jacob, D. J., Travnikov, O., Cuevas, C. A., Acuña, A. U., Rivero, D., Plane, J. M. C., Kinnison, D. E., and Sonke, J. E.: Photoreduction of gaseous oxidized mercury changes global atmospheric mercury speciation, transport and deposition, Nat Commun, 9, 4796, https://doi.org/10.1038/s41467-018-07075-3, 2018.

Salter, C., Tellinghuisen, P. C., Ashmore, J. G., and Tellinghuisen, J.: The emission spectrum of $^{200}Hg^{127}I$, J Mol Spectrosc, 120, 334–358, https://doi.org/10.1016/0022-2852(86)90009-3, 1986.

Schroeder, H. and Munthe, J.: Atmospheric Mercury-An Overview, Atmos Env, 32, https://doi.org/10.1016/S1352-2310(97)00293-8, 1998.

Shah, V., Jacob, D. J., Thackray, C. P., Wang, X., Sunderland, E. M., Dibble, T. S., Saiz-Lopez, A., Cernusák, I., Kellö, V., Castro, P. J., Wu, R., and Wang, C.: Improved mechanistic model of the atmospheric redox chemistry of mercury, Environ Sci Technol, 55, 14445–14456, https://doi.org/10.1021/ACS.EST.1C03160, 2021a.

Shah, V., Jacob, D. J., Thackray, C. P., Wang, X., Sunderland, E. M., Dibble, T. S., Saiz-Lopez, A., Cernusák, I., Kellö, V., Castro, P. J., Wu, R., and Wang, C.: Improved mechanistic model of the atmospheric redox chemistry of mercury, Environ Sci Technol, 55, 14445–14456, https://doi.org/10.1021/acs.est.1c03160, 2021b.

Shepler, B. C. and Peterson, K. A.: Mercury Monoxide: A Systematic Investigation of Its Ground Electronic State, J Phys Chem A, 107, 1783–1787, https://doi.org/10.1021/jp027512f, 2003.

Shepler, B. C., Balabanov, N. B., and Peterson, K. A.: Ab initio thermochemistry involving heavy atoms: an investigation of the reactions Hg + IX (X = I, Br, Cl, O)., J Phys Chem A, 109, 10363–72, https://doi.org/10.1021/jp0541617, 2005.

Sommar, J., Hallquist, M., Ljungström, E., and Lindqvist, O.: On the Gas Phase Reactions Between Volatile Biogenic Mercury Species and the Nitrate Radical, J Atmos Chem, 27, 233–247, https://doi.org/10.1023/A:1005873712847, 1997.

Sommar, J., Gårdfeldt, K., Strömberg, D., and Feng, X.: A kinetic study of the gas-phase reaction between the hydroxyl radical and atomic mercury, Atmos Environ, 35, 3049–3054, https://doi.org/10.1016/S1352-2310(01)00108-X, 2001.

Stanton, J. F.: On the vibronic level structure in the NO_3 radical. I. The ground electronic state, J Chem Phys, 126, https://doi.org/10.1063/1.2715547, 2007.

Stanton, J. F.: On the vibronic level structure in the NO_3 radical: II. Adiabatic calculation of the infrared spectrum, Mol Phys, 107, 1059–1075, https://doi.org/10.1080/00268970902740530, 2009.

Stanton, J. F. and Bartlett, R. J.: The equation of motion coupled-cluster method. A systematic biorthogonal approach to molecular excitation energies, transition probabilities, and excited state properties, J Chem Phys, 98, 7029–7039, https://doi.org/10.1063/1.464746, 1993.

Stanton, J. F. and Gauss, J.: Analytic energy derivatives for ionized states described by the equation-of-motion coupled cluster method, J Chem Phys, 101, 8938–8944, https://doi.org/10.1063/1.468022, 1994.

Stanton, J. F. and Gauss, J.: A simple scheme for the direct calculation of ionization potentials with coupled-cluster theory that exploits established excitation energy methods, J Chem Phys, 111, 8785–8788, https://doi.org/10.1063/1.479673, 1999.

Stanton, J. F., Gauss, J., and Bartlett, R. J.: Potential nonrigidity of the NO3 radical, J Chem Phys, 94, 4084–4087, https://doi.org/10.1063/1.460636, 1991.

Stanton, J. F., Gauss, J., Cheng, L., Harding, M. E., Matthews, D. A., and Szalay, P. Q.: CFOUR, Coupled-Cluster Techniques for Computational Chemistry, a Quantum-Chemical Program Package, http://www.cfour.de.

Sumner, A. L., Spicer, C. W., Satola, J., Mangaraj, R., Cowen, K. A., Landis, M. S., Stevens, R. K., and Atkeson, T. D.: Environmental Chamber Studies of Mercury Reactions in the Atmosphere, in: Dynamics of Mercury Pollution on Regional and Global Scales, Springer-Verlag, New York, 193–212, https://doi.org/10.1007/0-387-24494-8_9, 2005.

Viel, A. and Eisfeld, W.: NO_3 full-dimensional potential energy surfaces and ground state vibrational levels revisited, Chem Phys, 509, 81–90, https://doi.org/10.1016/J.CHEMPHYS.2018.01.003, 2018.

Wang, F., Saiz-Lopez, A., Mahajan, A. S., Gómez Martín, J. C., Armstrong, D., Lemes, M., Hay, T., and Prados-Roman, C.: Enhanced production of oxidised mercury over the tropical Pacific Ocean: a key missing oxidation pathway, Atmos Chem Phys, 14, 1323–1335, https://doi.org/10.5194/acp-14-1323-2014, 2014.

Weiss-Penzias, P., Jaffe, D. A., McClintick, A., Prestbo, E. M., and Landis, M. S.: Gaseous Elemental Mercury in the Marine Boundary Layer: Evidence for Rapid Removal in Anthropogenic Pollution, Environ Sci Technol, 37, 3755–3763, https://doi.org/10.1021/es0341081, 2003.

Wu, L., Mao, H., Ye, Z., Dibble, T. S., Saiz-Lopez, A., and Zhang, Y.: Improving Simulation of Gas-Particle Partitioning of Atmospheric Mercury Using CMAQ-newHg-Br v2, J Adv Model Earth Syst, 16, https://doi.org/10.1029/2023MS003823, 2024.

Wu, R., Wang, C., and Dibble, T. S.: First experimental kinetic study of the atmospherically important reaction of BrHg + NO_2, Chem Phys Lett, 759, 137928, https://doi.org/10.1016/j.cplett.2020.137928, 2020.

Wu, R., Castro, P. J., Gaito, C., Beiter, K., Dibble, T. S., and Wang, C.: Combined Experimental and Computational Kinetics Studies for the Atmospherically Important BrHg Radical Reacting with NO and O_2, J Phys Chem A, 126, 3914–3925, https://doi.org/10.1021/acs.jpca.2c02531, 2022.

Yanai, T., Tew, D. P., and Handy, N. C.: A new hybrid exchange–correlation functional using the Coulomb-attenuating method (CAM-B3LYP), Chem Phys Lett, 393, 51–57, https://doi.org/10.1016/j.cplett.2004.06.011, 2004.

Zhang, C. and Cheng, L.: Atomic Mean-Field Approach within Exact Two-Component Theory Based on the Dirac–Coulomb–Breit Hamiltonian, J Phys Chem A, 126, 4537–4553, https://doi.org/10.1021/acs.jpca.2c02181, 2022.

Zhao, Y. and Truhlar, D. G.: The M06 suite of density functionals for main group thermochemistry, thermochemical kinetics, noncovalent interactions, excited states, and transition elements: two new functionals and systematic testing of four M06-class functionals and 12 other functionals, Theor Chem Acc, 120, 215–241, https://doi.org/10.1007/s00214-007-0310-x, 2008.

Zhou, J. and Obrist, D.: Global Mercury Assimilation by Vegetation, Environ Sci Technol, 55, 14245–14257, https://doi.org/10.1021/ACS.EST.1C03530, 2021.